# CHAPTER 7

# The electromagnetic field coupling to buried wires: frequency and time domain analysis

D. Poljak
*Department of Electronics, FESB, University of Split, Split, Croatia.*

## Abstract

This chapter deals with the transient analysis of buried cables using the wire antenna theory and applying both the frequency and the time domain approach. On one hand, if the solution for a large number of incident waves arriving from various directions is of interest then the frequency domain approach is appropriate. On the other hand, for some electromagnetic compatibility applications in which accurate frequency data are required, the frequency samples obtained by the use of Fourier transform do not ensure accurate results and the time domain approach would be a better choice. Particularly, the direct time domain approach is convenient if the transient response is required only for the early time behavior, since the frequency domain approach requires computing of the frequency response up to the maximum effective frequency and the entire range of frequency spectrum has to be transformed. The frequency domain model is based on the Pocklington integral equation while the time domain formulation deals with the Hallen integral equation approach. Both the Pocklington and the Hallen equation are handled via the appropriate Galerkin–Bubnov scheme of the indirect boundary element method. The strengths and weaknesses of both approaches are discussed.

## 1 Introduction

The electromagnetic field coupling to lines buried in a lossy medium is of great practical interest for many electromagnetic compatibility (EMC) applications [1–4], such as transient analysis of power and communications cables. Basically, the buried wire can represent a telephone cable, power cable, or a cylindrical antenna operating at a very low frequency. Some important applications are also related to submarine communication (long dipoles submerged in water), geophysical

WIT Transactions on State of the Art in Science and Engineering, Vol 29, © 2008 WIT Press
www.witpress.com, ISSN 1755-8336 (on-line)
doi:10.2495/978-1-84564-063-7/07

probing and electromagnetic stimulation of biological tissue. In the past, the transient excitation of buried wires, as one of the major causes of malfunction of telecommunication and power lines, has been mostly related to the lightning discharge problems [3].

Generally, the electromagnetic field coupling to underground wires configurations [1, 2] has been investigated to a somewhat lesser extent than coupling to above-ground lines [3–11].

The studies related to buried wires are usually based on an approximate transmission line approach [3]. The transmission line approach can be considered as a compromise between a quasi-static approximation and a full wave (wire antenna) model, and it is mostly related to infinite or at least very long buried wires.

However, the effects at the line ends cannot be taken into account utilizing the transmission line approach [12]. Also, the effect of the earth–air interface has usually been neglected featuring the assumption that the wire is buried at a very large depth [1].

The transmission line approach, though sufficient approximation if long lines with electrically small cross sections are considered, fails if one deals with the lines of finite length and high-frequency excitations.

Namely, the transmission line model fails to predict resonances, fails to take into account the presence of a lossy ground and the effects at the line ends [3–7]. Consequently, when the lines of the finite length are of interest the full wave model based on the receiving antenna (scattering) theory has to be used.

Thus, the wave-like behavior of the induced responses at higher frequencies requires a more general approach which is based on integral equations arising from the wire antenna theory. On the other hand, the principal restriction of the wire antenna model applied to overhead lines is often related to the long computational time required for the calculations pertaining to the long lines.

The transient analysis of buried cables using the wire antenna theory can be carried out in either frequency or time domain. Essentially, there is no definitive advantage that could be gained using the indirect frequency domain approach or the direct time domain solution method.

Generally, if the solution for a large number of incident waves arriving from various directions is of interest then the frequency domain approach is appropriate.

On the other hand, for some EMC applications in which accurate frequency data are required, the frequency samples obtained by the use of Fourier transform do not ensure accurate results. The time domain approach would be a better choice if the transient response is required only for the early time behavior, since the frequency domain approach requires computing of the frequency response up to the maximum effective frequency and the entire range of frequency spectrum has to be transformed.

This chapter deals with both approaches. The frequency domain model is based on the Pocklington integral equation while the time domain formulation deals with the Hallen integral equation approach. The strengths and weaknesses of both approaches are discussed.

## 2 The frequency domain approach

The frequency domain antenna theory approach provides one to take into account the earth–air interface effects via rigorous Sommerfeld integral formulation. However, the Sommerfeld integrals cannot be evaluated analytically, while the corresponding numerical solution is rather demanding and very time consuming [13–17]. Consequently, some authors prefer to use a simplified approach based on the reflection coefficient approximation [1, 4].

The wire antenna approach to the analysis of the plane wave coupling to the buried cable of finite length, with the effect of the half space included via the reflection coefficient approximation, has been proposed in [18]. This approach has been extended to the more complex case of a plane wave excitation with an arbitrary angle of incidence [19].

The frequency domain formulation presented in this chapter is based on the Pocklington integro-differential equation. The reflection coefficient by which the earth–air interface is taken into account is included in the integral equation kernel.

This integral equation is solved via the Galerkin–Bubnov scheme of the indirect boundary element method (GB-IBEM) [20]. Furthermore, the transient response of the wire is computed using the inverse Fourier transform [21].

### 2.1 Formulation in the frequency domain

The horizontal line of length $L$ and radius $a$, buried in a lossy ground at depth $d$, is shown in Fig. 1. The current distribution along the buried wire is governed by the corresponding Pocklington integro-differential equation. This integro-differential equation can be derived by enforcing the interface conditions for the tangential electric field components.

Assuming the wire to be perfectly conducting, the total field along the wire surface vanishes, i.e.:

$$\vec{e}_x \vec{E}^{\,\mathrm{tot}} = 0 \tag{1}$$

where the total field $\vec{E}^{\,\mathrm{tot}}$ is composed from the excitation $\vec{E}^{\,\mathrm{exc}}$ and scattered field $\vec{E}^{\,\mathrm{sct}}$ field components, respectively:

$$\vec{E}^{\,\mathrm{tot}} = \vec{E}^{\,\mathrm{exc}} + \vec{E}^{\,\mathrm{sct}} \tag{2}$$

where the excitation field component represents the sum of the incident field $\vec{E}^{\,\mathrm{inc}}$ and field reflected from the lossy ground $\vec{E}^{\,\mathrm{ref}}$:

$$\vec{E}^{\,\mathrm{exc}} = \vec{E}^{\,\mathrm{inc}} + \vec{E}^{\,\mathrm{ref}} \tag{3}$$

The scattered field component is given by:

$$\vec{E}^{\,\mathrm{sct}} = -j\omega\vec{A} - \nabla\varphi \tag{4}$$

where $\vec{A}$ is the magnetic vector potential and $\varphi$ is the electric scalar potential.

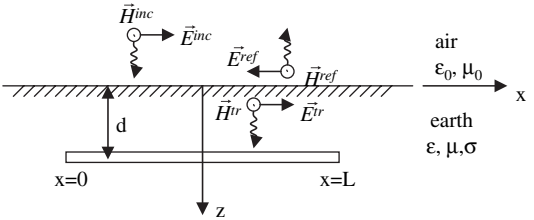


Figure 1: A straight wire of finite length buried in a dissipative medium.

According to the widely used thin wire approximation [3, 4] only the axial component of the magnetic potential differs from zero and eqn (4) becomes:

$$E_x^{\text{sct}} = -j\omega A_x - \frac{\partial \varphi}{\partial x} \tag{5}$$

where the magnetic vector potential and electric scalar potential are, respectively, defined as:

$$A_x = \frac{\mu}{4\pi} \int_0^L I(x')g(x,x')\,\mathrm{d}x' \tag{6}$$

$$\varphi(x) = \frac{1}{4\pi\varepsilon_{\text{eff}}} \int_0^L q(x')g(x,x')\,\mathrm{d}x' \tag{7}$$

where $\varepsilon_{\text{eff}}$ is the complex permittivity of the lossy ground given by:

$$\varepsilon_{\text{eff}} = \varepsilon_{\text{r}}\varepsilon_0 - j\frac{\sigma}{\omega} \tag{8}$$

while $q(x)$ is the charge distribution along the line, $I(x')$ denotes the induced current along the line and $g(x, x')$ stands for the Green's function given by:

$$g(x,x') = g_0(x,x') - R_{\text{TM}}g_i(x,x') \tag{9}$$

and $g_0(x, x')$ denotes the lossy medium Green function:

$$g_0(x,x') = \frac{\mathrm{e}^{-jk_2R_1}}{R_1} \tag{10}$$

while $g_i(x, x')$ is, in accordance to the image theory, given by:

$$g_i(x,x') = \frac{\mathrm{e}^{-jk_2R_2}}{R_2} \tag{11}$$

where $k_2$ is the propagation constant of the lower medium and $R_1$ and $R_2$ are distances from the source point in the ground and from the corresponding image in the air to the observation point defined by:

$$R_1 = \sqrt{(x-x')^2 + a^2}, \quad R_2 = \sqrt{(x-x')^2 + 4d^2} \tag{12}$$

The influence of a nearby ground interface is taken into account by means of the Fresnel plane wave reflection coefficient:

$$R_{\mathrm{TM}} = \frac{\frac{1}{\underline{n}}\cos\theta - \sqrt{\frac{1}{\underline{n}} - \sin^2\theta}}{\frac{1}{\underline{n}}\cos\theta + \sqrt{\frac{1}{\underline{n}} - \sin^2\theta}}, \quad \theta = \operatorname{arctg}\frac{|x-x'|}{2d}, \quad \underline{n} = \frac{\varepsilon_{\mathrm{eff}}}{\varepsilon_0} \tag{13}$$

The linear charge density and the current distribution along the line are related through the equation of continuity [7]:

$$q = -\frac{1}{j\omega}\frac{\mathrm{d}I}{\mathrm{d}x} \tag{14}$$

Substituting eqn (14) into eqn (7) yields:

$$\varphi\,(x) = -\frac{1}{j4\pi\omega\varepsilon_{\mathrm{eff}}}\int_0^L \frac{\partial I(x')}{\partial x'} g(x,x')\mathrm{d}x' \tag{15}$$

Combining eqns (5), (6) and (15) results in the following integral relationship for the scattered field:

$$E_x^{\mathrm{sct}} = -j\omega\frac{\mu}{4\pi}\int_0^L I(x')g(x,x')\mathrm{d}x' + \frac{1}{j4\pi\omega\varepsilon_{\mathrm{eff}}}\frac{\partial}{\partial x}\int_0^L \frac{\partial I(x')}{\partial x'} g(x,x')\mathrm{d}x' \tag{16}$$

Finally, eqns (3) and (16) result in the following integral equation for the unknown current distribution induced along the line:

$$E_x^{\mathrm{exc}} = j\omega\frac{\mu}{4\pi}\int_0^L I(x')g(x,x')\mathrm{d}x' - \frac{1}{j4\pi\omega\varepsilon_{\mathrm{eff}}}\frac{\partial}{\partial x}\int_0^L \frac{\partial I(x')}{\partial x'} g(x,x')\mathrm{d}x' \tag{17}$$

Integral equation (17) is well-known in antenna theory and represents one of the most commonly used variants of the Pocklington's integro-differential equation.

The electric field transmitted into the lossy ground and illuminating the buried line is given by:

$$E_x^{\mathrm{exc}} = E_x^{\mathrm{tr}} = E_0(\Gamma_{\mathrm{TE}}\sin\phi - \Gamma_{\mathrm{TM}}\cos\theta_t\cos\phi)\,\mathrm{e}^{-jk_2\vec{n}_t\vec{r}} \tag{18}$$

where $\alpha$ is the angle between *E-field* vector while the plane of incidence and $\theta_t$ is defined by the Snell's law [1]:

$$k_1\sin\theta = k_2\sin\theta_t \tag{19}$$

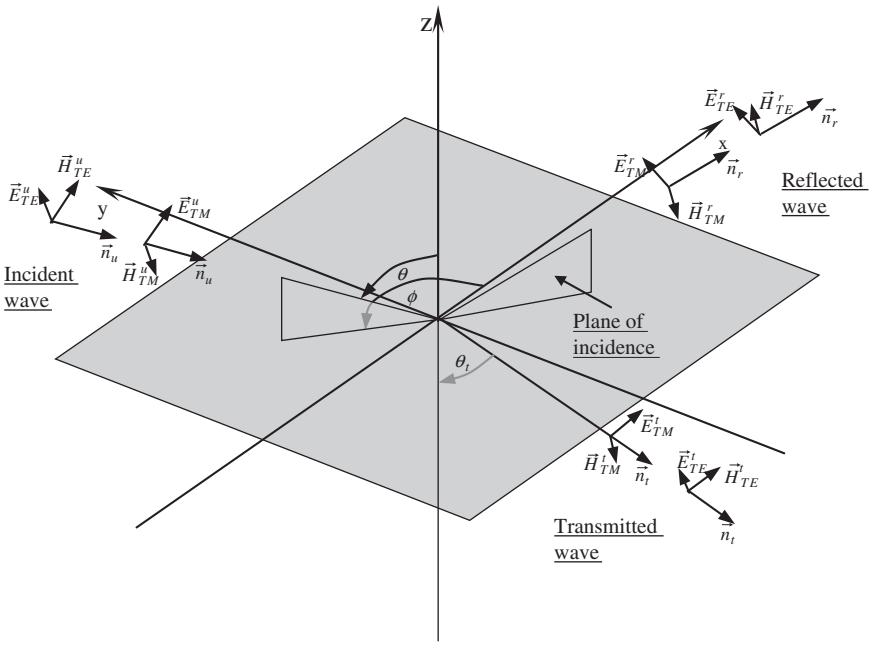


Figure 2: Incident, reflected and transmitted wave from an air–earth interface.

where $k_1$ is the propagation constant in the free space.

Quantities $\Gamma_{TM}$ and $\Gamma_{TE}$ denote the vertical and horizontal Fresnel transmission coefficients, respectively, at the air–earth interface (Fig. 2) given by [1]:

$$\Gamma_{TM} = \frac{2\sqrt{\underline{n}}\cos\theta}{\underline{n}\cos\theta + \sqrt{\underline{n} - \sin^2\theta}} \tag{20}$$

$$\Gamma_{TE} = \frac{2\cos\theta}{\cos\theta + \sqrt{\underline{n} - \sin^2\theta}} \tag{21}$$

and $\vec{n}_t\vec{r}$ is distance from the origin point to the observation point at the wire surface.

$$\vec{n}_t\vec{r} = -x\sin\theta_t\cos\phi - y\sin\theta_t\sin\phi - z\cos\theta_t \tag{22}$$

Solving the Pocklington integro-differential equation (17) the current distribution at the operating frequency is obtained.

### 2.2 Numerical solution of the integro-differential equation

The numerical solution of eqn (17) is obtained via GB-IBEM, which is outline below. More detailed description of the method can be found in [13].

An operator form of the Pocklington integro-differential equation (18) can be, for convenience, symbolically written as:

$$KI = E \tag{23}$$

where $K$ is a linear operator and $I$ is the unknown function to be found for a given excitation $E$.

The unknown current is expanded into a finite sum of linearly independent basis functions $\{f_i\}$ with unknown complex coefficients $\alpha_i$:

$$I \cong I_n = \sum_{i=1}^{n} \alpha_i f_i \tag{24}$$

Substituting eqn (24) into eqn (23) yields:

$$KI \cong KI_n = \sum_{i=1}^{n} \alpha_i K f_i = E_n = P_n(E) \tag{25}$$

where $P_n(E)$ is called a projection operator [13].

Now the residual $R_n$ is formed as follows:

$$R_n = KI_n - E = P_n(E) - E \tag{26}$$

According to the definition of the scalar product of functions in Hilbert function space the error $R_n$ is weighted to zero with respect to certain weighting functions $\{W_j\}$, i.e.:

$$\left\langle R_n, W_j \right\rangle = 0, \quad j = 1, 2, ..., n \tag{27}$$

where the expression in brackets stands for a scalar product of functions given by:

$$\left\langle R_n, W_j \right\rangle = \int_{\Omega} R_n W_j^{*} \, \mathrm{d}\Omega \tag{28}$$

where $\Omega$ denotes the actual calculation domain.

Since the operator $K$ is linear, a system of linear equations is obtained by choosing $W_j = f_j$, which implies the Galerkin–Bubnov procedure. Thus, it can be written as:

$$\sum_{i=1}^{n} \alpha_i \left\langle K f_i, f_j \right\rangle = \left\langle E, f_j \right\rangle, \quad j = 1, 2, ..., n \tag{29}$$

Equation (29) is the strong Galerkin–Bubnov formulation of the Pocklington integral equation (18). Utilizing the integral equation kernel symmetry and taking into

account the Dirichlet boundary conditions for the current at the wire ends of the cylinder, after integration by parts eqn (29) becomes:

$$\sum_{j=1}^{n} a_i \frac{1}{j4\pi\omega\varepsilon_{\text{eff}}}\left[\int_0^L \frac{\partial f_j(x)}{\partial x}\int_0^L \frac{\partial f_i(x')}{\partial x'} g(x,x')\mathrm{d}x'\,\mathrm{d}x + k_2^2\int_0^L f_j(x)\int_0^L f_i(x')g(x,x')\mathrm{d}x'\,\mathrm{d}x\right]$$
$$= \int_0^L E_x^{\text{exc}}(x) f_j(x)\,\mathrm{d}x, \quad j = 1,2,\ldots n \tag{30}$$

Equation (30) represents the weak Galerkin–Bubnov formulation of the integral equation (23).

The resulting system of algebraic equations arising from the boundary element discretization of eqn (30) is given by:

$$\sum_{j=1}^{M} [Z]_{ji}\{I\}_i = \{V\}_j, \quad j = 1,2,...,M \tag{31}$$

where $[Z]_{ji}$ is the local matrix representing the interaction of the $i$th source boundary element with the $j$th observation boundary element:

$$[Z]_{ji} = \frac{1}{j4\pi\omega\varepsilon_{\text{eff}}}\left[\int_0^L \{D\}_j\int_0^L \{D\}^{\mathrm{T}} g(x,x')\mathrm{d}x'\,\mathrm{d}x + k_2^2\int_0^L \{f\}_j\int_0^L \{f'\}^{\mathrm{T}} g(x,x')\mathrm{d}x'\,\mathrm{d}x\right] \tag{32}$$

The vector $\{I\}$ contains the unknown coefficients of the solution, and it represents the local voltage vector. Matrices $\{f\}$ and $\{f'\}$ contain the shape functions while $\{D\}$ and $\{D'\}$ contain their derivatives, $M$ is the total number of line segments, and $\Delta l_i$, $\Delta l_j$ are the widths of $i$th and $j$th segment.

Functions $f_k(z)$ are the Lagrange's polynomials and $\{V\}_j$ is the local right-side vector for the $j$th observation segment,

$$\{V\}_j = \int_{\Delta l_j} E_x^{\text{exc}}\{f\}_j\,\mathrm{d}z \tag{33}$$

representing the local voltage vector.

Linear approximation over a boundary element is used as it has been shown that this choice provides accurate and stable results [13].

### 2.3 The calculation of a transient response

Calculating the current distribution along a buried wire in a wide frequency spectrum one obtains the transfer function of the system, $H(f)$ is obtained.

To analyze the transient response of the buried wire, an incident field in a form of a single exponentially decaying function is used:

$$e_x^{\mathrm{tr}}(t) = E_0 e^{-at} \tag{34}$$

which Fourier transform is given by:

$$E_x^{\mathrm{tr}}(f) = \frac{E_0}{a + j2\pi f} \tag{35}$$

Now, the current distribution $I(f)$, i.e. the frequency response of the wire to the particular excitation (35) is obtained by multiplying the frequency spectrum of the excitation function with the corresponding transfer function of the linear system $H(f)$:

$$I(f) = H(f)E_x^{\mathrm{tr}}(f) \tag{36}$$

Applying the inverse Fourier transform is to be applied to the function $I(f)$ yields the transient current induced along the buried transmission line [21]:

$$i(t) = \int_{-\infty}^{\infty} I(f)e^{j2\pi ft}\mathrm{d}\omega \tag{37}$$

As the system transfer function $H(f)$ is represented by the discrete set of values, and the actual frequency response $I(f)$ is also represented by a discrete set of values, the integral equation (37) thus cannot be solved analytically and one has to deal with the Discrete Fourier transform (or in this case Fast Fourier Transform), i.e.:

$$i(t) = \mathrm{IFFT}(I(f)) \tag{38}$$

Thus, the discrete set of the time domain current values is defined by [21]:

$$i(n\Delta t) = F\sum_{k=0}^{N-1} I(k\,\Delta f)e^{jk\,\Delta f\,n\,\Delta t} \tag{39}$$

where $F$ is the highest frequency taken into account, $N$ is the total number of frequency samples, $\Delta f$ is sampling interval and $\Delta t$ is the time step.

### 2.4 Numerical results

For the comparison purposes, first the current distribution induced along a wire conducting cylinder, immersed in sea water, is computed assuming a unit incident field. The water parameters are $\varepsilon_r = 80$ and $\sigma = 4$ S/m, and the operating frequency is $f = 1$ MHz. The cylinder length is $L = 120$ and 160 m, respectively, with a radius of $a = 0.6$ and 0.8 m, respectively, while in Fig. 3 the calculated current distributions are compared to the analytical results available from [22]. Agreement is found to be satisfactory.

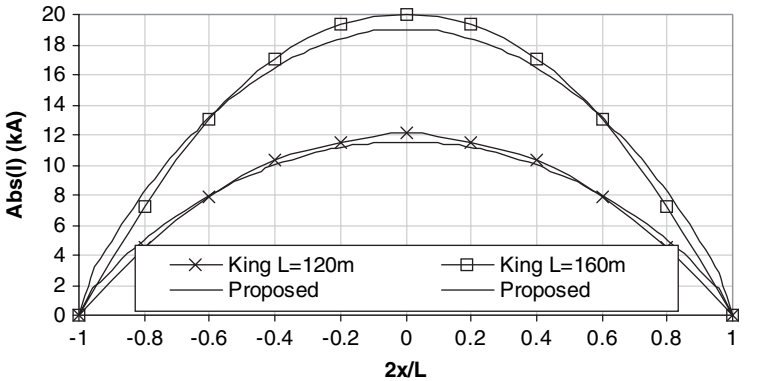


Figure 3: Comparison of numerical results obtained with different solution methods.

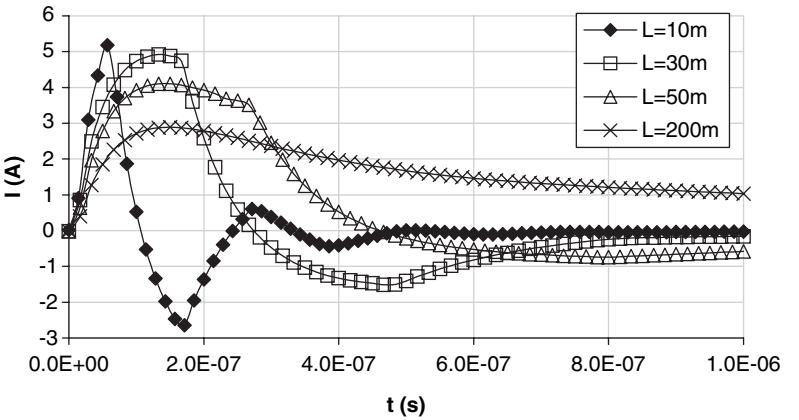


Figure 4: Transient response for different wire lengths.

Further numerical examples are related to the transmission lines buried in a lossy ground with permittivity $\varepsilon_r = 10$ and conductivity $\sigma = 0.001$ S/m. Conductor radius is $a = 1$ cm wire length $L$ and burial depth $d$ are varied. The wire is excited by the transmitted plane wave with a single exponential decaying form eqn (35). The parameters of the exponential function are, as follows: $E_0 = 1$ V/m, $a = (7.854 \times 10^{-8}\ \text{s})^{-1}$.

The transient response, i.e. the current induced at the center of the wires having various lengths for the normal incidence is shown in Fig. 4. The burial depth is $d = 1$ m. The current wave reflections from the wire ends are clearly visible, particularly for the shorter wires. Figure 5 shows the influence of the burial depth on the induced current at the center of the 200 m long wire.

The both time shift and the attenuation of the signal seems to be increased with the depth. The only exception occurs for $d = 0.1$ m, where the induced current is lower then for $d = 1$ m. This happens due to the vicinity of the nearby ground–air interface.

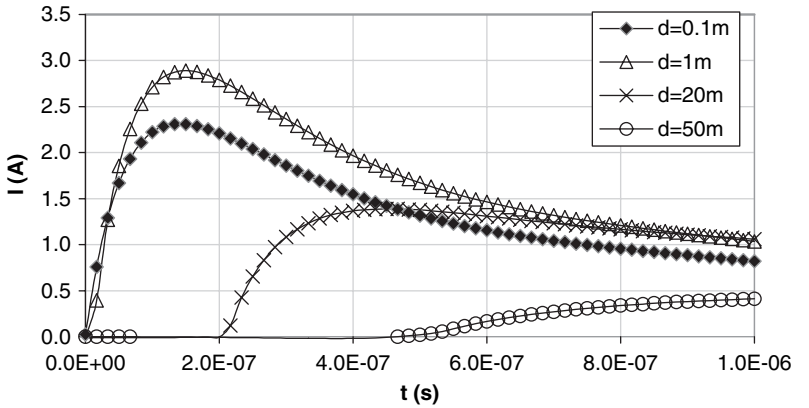


Figure 5: Transient response for different burial depths.

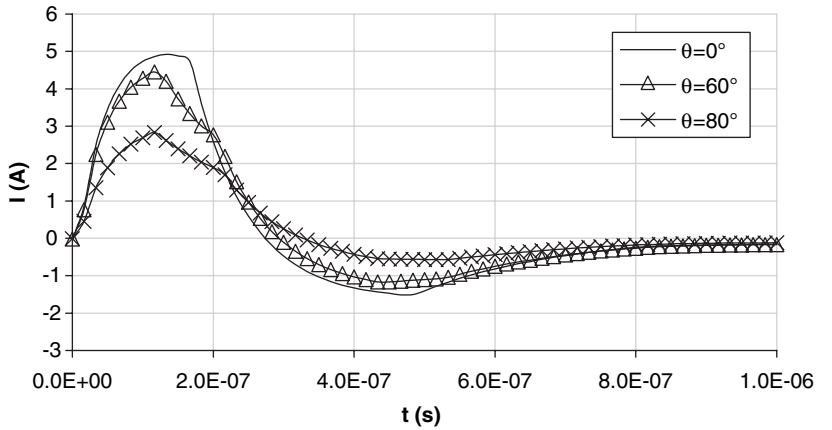


Figure 6: Transient response for different angles of incidence.

The transient response of the wire of the transmission line of length $L = 30$ m buried at depth $d = 1$ m for various angles of incidence $\theta = 0°$, 60° and 80° is shown in Fig. 6.

The transient response of the wire of the transmission line of length $L = 30$ m buried at depth $d = 1$ m for various angles of incidence $\theta = 0°$, 60° and 80° is shown in Fig. 6. For the higher angle $\theta$, amplitude of the induced current at the wire center is smaller, since the tangential component of the transmitted electric field is also decreased.

## 3 Time domain approach

This section deals with a time domain study of a single straight wire embedded in a dielectric half-space and illuminated by a non-uniform transient electric field.

This topic is very important as a starting point in the transient analysis of wires buried in a lossy medium which is of great practical interest for many EMC applications [1–4].

The analysis presented in this section is based on the wire antenna theory and is carried out directly in the time domain. Dealing with a rather simple geometry of a single wire embedded in a dielectric half-space this section aims to introduce some basic ideas on the subject. The method can be also applied to a case of arbitrary wire configurations, which is of much more practical importance in EMC applications.

The time domain formulation presented in this section is based on the space–time Hallen integral equation for half-space problems [23]. The effects of the two-media configuration are taken into account via the corresponding reflection coefficient and the transmission coefficient. The transient current along the straight wire embedded in a dielectric half-space is obtained by solving the corresponding Hallen integral equation via the time domain variant of the GB-IBEM [13].

Once calculating the space–time current distribution along the wire, to further evaluate the obtained transient response, the time domain energy measures can be computed by spatially integrating the squared current and charge along the wire [24–27].

Furthermore, a simplified version of space–time reflection/transmission coefficient has been promoted in [28], while an alternative formulation for a finite length wire placed within the dielectric half-space featuring the simplified form of the reflection/transmission coefficient, instead of use of Fresnel coefficients has been proposed in [29].

This alternative approach to the time domain analysis of buried wires is presented in this section, as well.

### 3.1 Formulation in the time domain

A perfectly conducting straight thin wire of length $L$ and radius $a$, immersed in a dielectric medium at depth $d$ is considered, as shown in Fig. 7. The wire is illuminated by a horizontally polarized transient electric field tangential along its

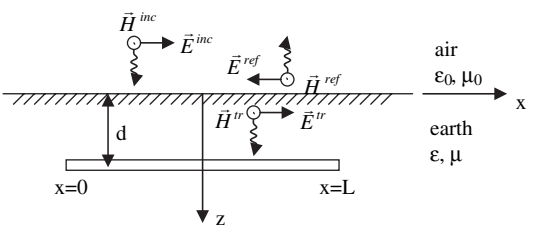


Figure 7: A straight wire embedded in a dielectric half-space.

surface, i.e. the case of normal incidence is considered only.

The mathematical framework of the problem is based on the wire antenna theory and thin wire approximation [3, 4].

The transient induced current flowing along the straight wire embedded in a dielectric half-space is governed by the corresponding space–time integral equation. The time domain formulation for the single wire problem in terms of the Pocklington or the Hallen integral equation type can be readily obtained as an extension of the wire in homogeneous dielectric medium.

The time domain Pocklington type integral equations often suffer from numerical instabilities, i.e. from the non-physical, rapidly growing oscillations at later instants of time [30].

On the other hand, the time domain Hallen integral equation does not contain either space or time derivatives within its kernel, which are found to be the origin of numerical instabilities. Consequently, the Hallen equation has been proven to be attractive from the computational point of view [4, 30–32].

The Hallen integral equation approach, also used for the transient analysis of straight wire configuration above-ground [8–11], is applied to the problem of wires embedded in a dielectric half-space in this section. The Hallen integral equation for the straight wire in unbounded lossless medium can be readily derived from the corresponding Pocklington integro-differential equation type.

Since the wire is perfectly conducting the tangential component of the total field vanishes on the antenna surface, i.e.:

$$E_x^{\text{inc}} + E_x^{\text{sct}} = 0 \tag{40}$$

where $E_x^{\text{inc}}$ is the incident and $E_x^{\text{sct}}$ scattered field on the metallic wire surface. From the first Maxwell equation:

$$\nabla x \vec{E} = -\frac{\partial \vec{B}}{\partial t} \tag{41}$$

and using the vector magnetic potential $\vec{A}$:

$$\vec{B} = \nabla x \vec{A} \tag{42}$$

it follows:

$$\vec{E}^{\text{inc}}\big|_{\text{tan}} = \left(\frac{\partial \vec{A}}{\partial t} + \nabla\varphi\right)\Big|_{\text{tan}} \tag{43}$$

where $\vec{A}$ and $\varphi$ are space–time-dependent magnetic vector and electric scalar potential, respectively. These two potentials are to satisfy the Lorentz gauge:

$$\frac{\partial \varphi}{\partial t} + \frac{1}{\mu\varepsilon}\nabla\vec{A} = 0 \tag{44}$$

Differentiating eqn (43) and taking into account the Lorentz gauge equation (44) yields in the wave equation for magnetic vector potential $\vec{A}$:

$$\left(\frac{\partial^2 \vec{A}}{\partial t^2} - \frac{1}{\mu\varepsilon}\nabla(\nabla\vec{A})\right)_{|_{\tan}} = \frac{\partial \vec{E}^{\,\mathrm{inc}}}{\partial t}_{|_{\tan}} \tag{45}$$

In accordance to the thin wire approximation, only the axial component of the vector potential exists, so it can be written:

$$\frac{\partial^2 A_x}{\partial x^2} - \frac{1}{v^2}\frac{\partial^2 A_x}{\partial t^2} = -\frac{\partial E_x^{\mathrm{inc}}}{\partial t} \tag{46}$$

where $v$ is the velocity of wave propagation in a homogeneous dielectric medium, defined as follows:

$$v = \frac{1}{\sqrt{\mu\varepsilon_{rg}\varepsilon_0}} \tag{47}$$

where $\varepsilon_{\mathrm{rg}}$ is the lower medium relative permittivity where $c$ denotes the velocity of light.

Equation (46) is valid on the surface of the perfect conductor and the solution can be represented by a sum of the homogeneous equation solution and particular solution of the inhomogeneous equation:

$$A_x(x,t) = A_x^{\mathrm{h}}(x,t) + A_x^{\mathrm{p}}(x,t) \tag{48}$$

In addition, the solution of the homogeneous wave equation is given as a superposition of incident and reflected wave [13]:

$$A_x^{\mathrm{h}}(x,t) = F_1\left(t - \frac{x}{v}\right) + F_2\left(t + \frac{x}{v}\right) \tag{49}$$

The particular solution is given by the integral [13]:

$$A_x^{\mathrm{p}}(x,t) = \frac{\varepsilon v}{2}\int_{-\infty}^{x}\int_{-\infty}^{t-\frac{(x-x')}{c}} \frac{\partial E_x^{\mathrm{inc}}(x',t')}{\partial t}\mathrm{d}t'\,\mathrm{d}x' + \frac{\varepsilon v}{2}\int_{-\infty}^{x}\int_{-\infty}^{t+\frac{(x-x')}{c}} \frac{\partial E_x^{\mathrm{inc}}(x',t')}{\partial t}\mathrm{d}t'\,\mathrm{d}x' \tag{50}$$

Since the differential equation is related to the wire antenna surface eqn (50) simplifies into:

$$A_x^{\mathrm{p}}(x,t) = \frac{1}{2Z_{\mathrm{g}}}\int_0^L E_x^{\mathrm{inc}}\left(x', t - \frac{|x-x'|}{v}\right)\mathrm{d}x' \tag{51}$$

where $Z_{\mathrm{g}}$ is the corresponding impedance of a dielectric medium given by:

$$Z_{\mathrm{g}} = \sqrt{\frac{\mu}{\varepsilon_{rg}\varepsilon_0}} \tag{52}$$

On the other hand, the magnetic vector potential on the metallic wire surface on the left-hand side of eqn (48) may be also obtained as a solution of the wave equation:

$$\nabla^2\vec{A} - \mu\varepsilon\frac{\partial^2\vec{A}}{\partial t^2} = -\mu\vec{J}(r,t) \tag{53}$$

where $\vec{J}(r,t)$ denotes the surface current density.

The solution of differential equation (53) is usually obtained via the Green function theory by introducing the auxiliary equation:

$$\nabla^2 g - \mu\varepsilon\frac{\partial^2 g}{\partial t^2} = \delta(\vec{r}-\vec{r}', t-t') \tag{54}$$

The solution is given in the form of retarded Dirac impulse:

$$g(\vec{r}-\vec{r}', t-t') = \frac{\delta(t-t'-(R/v))}{4\pi R} \tag{55}$$

where $R$ is a distance from the source to the observation point.

Then the solution of eqn (53) using the Green function approach may be written in the form:

$$\vec{A}(r,t) = \frac{\mu}{4\pi}\int_{-\infty}^{t}\int_{S}\vec{J}_s(\vec{r}',t)\frac{\delta(t-t'-R/v)}{R}\,\mathrm{d}S'\,\mathrm{d}t' \tag{56}$$

Performing the time domain integration one obtains:

$$\vec{A}(r,t) = \frac{\mu}{4\pi}\iint_{S}\frac{\vec{J}_s(r',t-R/v)}{R}\,\mathrm{d}S' \tag{57}$$

According to the thin wire approximation, the equivalent current along the wire is assumed to flow in the axis, while the observation points are located on the antenna surface, i.e. it follows:

$$I(x,t) = 2\pi a J_z(x,t) \tag{58}$$

and the axial component of the magnetic vector potential is given by:

$$A_x(x,t) = \frac{\mu}{4\pi}\int_0^L \frac{I(x',t-R/v)}{R}\,\mathrm{d}x' \tag{59}$$

Combining the relations (46) and (59) yields the Pocklington integro-differential equation:

$$\left[\frac{\partial^2}{\partial x^2} - \frac{1}{v^2}\frac{\partial^2}{\partial t^2}\right]\int_0^L \frac{I(x',t-R/v)}{4\pi R}\,\mathrm{d}x' = \frac{\partial E_x^{\mathrm{inc}}}{\partial t} \tag{60}$$

while relations (48), (49), (51) and (59) leads to the space–time Hallen integral equation:

$$\int_0^L \frac{I(x',t-R/v)}{4\pi R}\,\mathrm{d}x' = F_0\left(t-\frac{x}{v}\right)+F_L\left(t-\frac{L-x}{v}\right)+\frac{1}{2Z_\mathrm{g}}\int_0^L E_x^{\mathrm{inc}}\left(x',t-\frac{|x-x'|}{v}\right)\mathrm{d}x' \tag{61}$$

Equations (60) and (61) are both related to the straight, finite length wire in an unbounded dielectric medium, where the distance from the observation point is given by:

$$R=\sqrt{(x-x')^2+a^2} \tag{62}$$

The multiple reflections of the current at the free ends of the wire are taken into account by the unknown functions $F_0(t)$ and $F_L(t)$.

The Hallen integral equation for a homogeneous lossless medium can be also derived directly from the Pocklington equation by performing the straight-forward convolution [10].

The corresponding Hallen integral equation for the wire embedded in a dielectric half-space can be derived gradually.

As a first step, the Hallen integral equation for an unbounded medium equation (61) is transferred into the frequency domain:

$$\int_0^L \frac{I(x',s)\mathrm{e}^{-sR/v}}{4\pi R}\,\mathrm{d}x' = F_0(s)\mathrm{e}^{-sX/v}+F_L(s)\mathrm{e}^{-s(L-X)/v}+\frac{1}{2Z_\mathrm{g}}\int_0^L E_x^{\mathrm{inc}}(x',s)\,\mathrm{e}^{-s(|x-x'|/v)}\,\mathrm{d}x' \tag{63}$$

where $s=j\omega$ denotes the Laplace variable.

The frequency domain Hallen integral equation for a straight wire in a dielectric half-space is obtained by extending the integral equation (63) with an additional term due to an image wire in the air located at height $d$ above interface. This term contains the reflection coefficient $\Gamma_{\mathrm{ref}}$ for the transverse magnetic (TM) polarization multiplied by the Green function of the image wire in the air. In addition, the incident field $E_x^{\mathrm{inc}}$ appearing in the last term in eqn (61) has to be replaced by the corresponding transmitted field $E_x^{\mathrm{tr}}$.

Thus, the resulting space frequency Hallen integral equation for the straight wire embedded in a dielectric medium becomes:

$$\begin{aligned}&\int_0^L \frac{I(x',s)\,\mathrm{e}^{-\frac{sR}{v}}}{4\pi R}\,\mathrm{d}x' - \int_0^L \Gamma_{\mathrm{ref}}(\theta)\frac{I(x',s)\mathrm{e}^{-\frac{sR^*}{v}}}{4\pi R^*}\,\mathrm{d}x' \\ &\quad = F_0(s)\,\mathrm{e}^{-\frac{sx}{v}}+F_L(s)\,\mathrm{e}^{-s\frac{(L-x)}{v}}+\frac{1}{2Z_\mathrm{g}}\int_0^L E_x^{\mathrm{tr}}(x',s)\,\mathrm{e}^{-s\frac{|x-x'|}{v}}\mathrm{d}x'\end{aligned} \tag{64}$$

where $R^*$ is the distance from the source point located at the image wire in the air to the observation point located at the wire immersed in a dielectric medium:

$$R^* = \sqrt{(x-x')^2 + 4d^2} \tag{65}$$

The space dependent reflection coefficient, by which the ground–air interface effects are taken into account, is defined by the relation [1]:

$$\Gamma_{\text{ref}}(\theta) = \frac{\dfrac{1}{\varepsilon_{\text{rg}}}\cos\theta - \sqrt{\dfrac{1}{\varepsilon_{\text{rg}}} - \sin^2\theta}}{\dfrac{1}{\varepsilon_{\text{rg}}}\cos\theta + \sqrt{\dfrac{1}{\varepsilon_{\text{rg}}} - \sin^2\theta}}, \quad \theta = \text{arctg}\frac{|x-x'|}{2d} \tag{66}$$

Finally, the electric field transmitted into the dielectric medium $E_x^{\text{tr}}$ is given as follows:

$$E_x^{\text{tr}} = \Gamma_{\text{tr}}(\theta_{\text{tr}}) E_x^{\text{inc}} \tag{67}$$

where $E_x^{\text{inc}}$ is the incident field in the air and $\Gamma_{\text{tr}}(\theta_{\text{tr}})$ is the corresponding transmission coefficient by which the air–ground interface effects are taken into account.

The space dependent transmission coefficient, for the case of normal incidence considered in this work, is given by [23]:

$$\Gamma_{\text{tr}}(\theta_{\text{tr}}) = \left.\frac{2\sqrt{\varepsilon_{\text{rg}}}\cos\theta_{\text{tr}}}{\varepsilon_{\text{rg}}\cos\theta_{\text{tr}} + \sqrt{\varepsilon_{\text{rg}} - \sin^2\theta_{\text{tr}}}}\right|_{\theta_{\text{tr}}=0} = \frac{2}{\sqrt{\varepsilon_{\text{rg}}}+1} \tag{68}$$

where $\theta_{\text{tr}}$ is the angle of transmission.

The time domain Hallen equation for a straight thin wire in a dielectric half-space now can be obtained applying the inverse Laplace transform and the convolution theorem to the integral equation (64).

Therefore, it follows:

$$\int_0^L \frac{I(x',t-R/v)}{4\pi R}\,\mathrm{d}x' - \int_{-\infty}^{t}\int_0^L \Gamma_{\text{ref}}(\theta,\tau)\frac{I(x',t-R^*/v-\tau)}{4\pi R^*}\,\mathrm{d}x'\,\mathrm{d}\tau$$
$$= F_0\left(t-\frac{x}{v}\right) + F_L\left(t-\frac{L-x}{v}\right) + \frac{1}{2Z_{\text{g}}}\int_0^L E_x^{\text{tr}}\left(x', t-\frac{|x-x'|}{v}\right)\mathrm{d}x' \tag{69}$$

where the time domain counterpart of the Fresnel reflection coefficient $\Gamma_{\text{ref}}(\theta, t)$ is:

$$\Gamma_{\text{ref}}(\theta,t) = \Gamma_{\text{ref}}(\theta)\delta(t) \tag{70}$$

and $\delta(t)$ stands for the Dirac impulse.

The transmitted electric field in the dielectric medium $E_x^{\text{tr}}$ represents a time domain counterpart of the relation (67) and can be obtained from the convolution integral:

$$E_x^{\text{tr}}(x,t) = \int_{-\infty}^{t} E_x^{\text{inc}}(x, t-\tau)\Gamma_{\text{tr}}(\theta_{\text{tr}}, \tau)\mathrm{d}\tau \tag{71}$$

where $\Gamma_{\text{tr}}(\theta_{\text{tr}}, t)$ is the time domain transmission coefficient counterpart of the expression (68):

$$\Gamma_{\text{tr}}(\theta, t) = \Gamma_{\text{tr}}(\theta)\delta(t) \tag{72}$$

Substituting the relations (72) and (68) into eqn (71), for the case of normal incidence ($\theta_{\text{tr}} = 0$), it follows:

$$E_x^{\text{tr}} = \frac{2}{\sqrt{\varepsilon_{\text{rg}}} + 1} E_x^{\text{inc}}(t - t_0) \tag{73}$$

where $t_0 = d/v$ denotes the time delay.

It should be stated that a field reference point ($x = 0$, $z = 0$) has been used throughout this analysis.

Finally, combining the relations (66)–(73) the resulting integral equation for the wire immersed in a dielectric medium becomes:

$$\int_0^L \frac{I(x', t - R/v)}{4\pi R}\mathrm{d}x' - \int_0^L \frac{\dfrac{1}{\varepsilon_{\text{rg}}}\cos\theta - \sqrt{\dfrac{1}{\varepsilon_{\text{rg}}} - \sin^2\theta}}{\dfrac{1}{\varepsilon_{\text{rg}}}\cos\theta + \sqrt{\dfrac{1}{\varepsilon_{\text{rg}}} - \sin^2\theta}} \frac{I(x', t - R^*/v)}{4\pi R^*}\mathrm{d}x'$$

$$= F_0\left(t - \frac{x}{v}\right) + F_L\left(t - \frac{L-x}{v}\right) + \frac{1}{2Z_{\text{g}}}\int_0^L \frac{2}{\sqrt{\varepsilon_{\text{rg}}} + 1} E_x^{\text{inc}}\left(x', t - t_0 - \frac{|x - x'|}{v}\right)\mathrm{d}x' \tag{74}$$

The problem of a straight wire embedded in a dielectric medium governed by the space–time Hallen integral equation (74) can be solved by prescribing, without any loss of generality, the zero edge $I(0, t) = I(L, t) = 0$ and initial conditions $I(x, 0) = 0$.

The use of a convolution approach through eqns (69)–(72) to handle the reflection and transmission coefficients is not necessary for the case of dielectric half-space as they are only functions of angle. This integral equation formulation is used as it can serve as a starting point in deriving the model for the wire buried in a medium with finite conductivity.

### 3.2 Time domain energy measures

The transient response of a straight thin wire embedded in a dielectric half-space can be postprocessed by the time domain energy measures based on spatial integrals of the squared current and charge induced along the wire.

The time domain energy measures represented by the current and charge induced on an object yield insight into where and how much the object radiates as a function of time. These measures were originally proposed in [24], for wires in free space, and re-examined in [10, 25] and recently in [26]. The concept of the time domain energy measures is extended to the case of buried wires in [27].

Upon solving the set of Hallen integral equations (74) for the transient current along the wire located in a dielectric medium, the charge distribution along the wire can be determined from the continuity equation [10]:

$$q = -\int_0^t \frac{\partial I(x',t)}{\partial x'} \mathrm{d}t \tag{75}$$

where $q$ is the linear charge distribution along the embedded wire in a dielectric half-space.

Having found the current and charge, measures of the $H$-field (kinetic) and the $E$-field (static) energy densities are expressed as proposed in [27].

The $H$-field energy is represented by the relation:

$$W_I = \frac{\mu_0}{4\pi} \int_0^L I^2(x',t) \mathrm{d}x' \tag{76}$$

while the $E$-field energy is measured by the following integral:

$$W_q = \frac{1}{4\pi\varepsilon_r\varepsilon_0} \int_0^L q^2(x',t) \mathrm{d}x' \tag{77}$$

The total energy stored in the near field is proportional to the sum of $W_I$ and $W_q$ [27].

Numerical procedures for the calculation of the current, charge and time domain energy are outlined in Section 2.3.

### 3.3 Time domain numerical solution procedures

Time domain modeling is a more demanding task than is the frequency domain approach however the former provides not only a better insight into the physical transient phenomena, but also some computational advantages [4, 10, 14]. The time domain version of the GB-IBEM applied to the solution of various Hallen integral equation types provides the stable numerical results [8–11] and it is used for numerical handling of the straight thin wire in a dielectric half-space in [23].

As the time domain solution procedure for the Hallen integral equation is stable for an arbitrary time interval, it does not require any smoothing procedure, contrary to the most of the known techniques [30]. The space–time discretization is performed carefully, so that within one time increment the propagation on at least one space segment is considered, thus satisfying the inequality:

$$\Delta t \leq \frac{\Delta z}{c} \tag{78}$$

Through the marching-on-in-time procedure it is possible to obtain the solution for the current at a present time for each space node as a function of currents at previous instants, without requiring matrix inversion. It is also necessary to prescribe the initial values of current at the wire ends to start the stepping procedure.

According to the usual space–time discretization procedure, the local approximation for unknown current can be expressed in the form:

$$I(x',t') = \{f\}^{\mathrm{T}}\{I\} \tag{79}$$

where $\{f\}$ is a vector containing shape functions, and $\{I\}$ is the time-dependent solution vector. In addition, applying the weighted residual approach, the space boundary discretization of integral equation (74) leads to the local equation system for *i*th source and *j*th observation boundary element:

$$\begin{aligned}
&\int_{\Delta l_j}\int_{\Delta l_i}\{f\}_j\{f\}_i^{\mathrm{T}}\frac{1}{4\pi R}\mathrm{d}x'\,\mathrm{d}x\{I\}\Big|_{t-\frac{R}{v}} \\
&\quad-\int_{\Delta l_j}\int_{\Delta l_i}\{f\}_j\{f\}_i^{\mathrm{T}}\frac{\dfrac{1}{\varepsilon_{\mathrm{rg}}}\cos\theta-\sqrt{\dfrac{1}{\varepsilon_{\mathrm{rg}}}-\sin^2\theta}}{\dfrac{1}{\varepsilon_{\mathrm{rg}}}\cos\theta+\sqrt{\dfrac{1}{\varepsilon_{\mathrm{rg}}}-\sin^2\theta}}\frac{1}{4\pi R^*}\mathrm{d}x'\,\mathrm{d}x\{I\}\Big|_{t-\frac{R^*}{v}} \\
&=\int_{\Delta l_j}F_0\left(t-\frac{x}{v}\right)\{f\}_j\mathrm{d}x+\int_{\Delta l_j}F_L\left(t-\frac{L-x}{v}\right)\{f\}_j\mathrm{d}x \\
&\quad+\frac{1}{2Z_{\mathrm{g}}}\int_{\Delta l_j}\int_{\Delta l_i}\frac{2}{\sqrt{\varepsilon_{\mathrm{rg}}}+1}E_x^{\mathrm{inc}}\left(x',t-t_0-\frac{|x-x'|}{c}\right)\{f\}_j\mathrm{d}x'\,\mathrm{d}x
\end{aligned} \tag{80}$$

Expression (80) can be written in the matrix form given by:

$$\begin{aligned}
&[A]\{I\}\Big|_{t-\frac{R}{c}}-[A_1^*]\{I\}\Big|_{t-\frac{R^*}{c}}=[B]\{E\}\Big|_{t-\frac{|x-x'|}{c}}+[C]\left\{\sum_{n=0}^{\infty}I^n\right\}\Big|_{t-\frac{x}{c}-\frac{2nL}{c}-\frac{R_0}{c}} \\
&-[C_1^*]\left\{\sum_{n=0}^{\infty}I^n\right\}\Big|_{t-\frac{x}{c}-\frac{2nL}{c}-\frac{R_0^*}{c}}-[B]\left\{\sum_{n=0}^{\infty}E^n\right\}\Big|_{t-\frac{x}{c}-\frac{2nL}{c}-\frac{x'}{c}}-[D]\left\{\sum_{n=0}^{\infty}I^n\right\}\Big|_{t-\frac{x}{c}-\frac{2n+1}{c}L-\frac{R_L}{c}} \\
&+[D_1^*]\left\{\sum_{n=0}^{\infty}I^n\right\}\Big|_{t-\frac{x}{c}-\frac{2n+1}{c}L-\frac{R_L^*}{c}}+[B]\left\{\sum_{n=0}^{\infty}E^n\right\}\Big|_{t-\frac{x}{c}-\frac{2n+1}{c}L-\frac{L-x'}{c}}+[D]\left\{\sum_{n=0}^{\infty}I^n\right\}\Big|_{t-\frac{L-x}{c}-\frac{2nL}{c}-\frac{R_L}{c}}
\end{aligned}$$

$$-[D_1^*]\left\{\sum_{n=0}^{\infty} I^n\right\}\Bigg|_{t-\frac{L-x}{c}-\frac{2nL}{c}-\frac{R_L^*}{c}} -[B]\left\{\sum_{n=0}^{\infty} E^n\right\}\Bigg|_{t-\frac{L-x}{c}-\frac{2nL}{c}-\frac{L-x'}{c}} -[C]\left\{\sum_{n=0}^{\infty} I^n\right\}\Bigg|_{t-\frac{L-x}{c}-\frac{2n+1}{c}L-\frac{R_0}{c}}$$
$$+[C_1^*]\left\{\sum_{n=0}^{\infty} I^n\right\}\Bigg|_{t-\frac{L-x}{c}-\frac{2n+1}{c}L-\frac{R_0^*}{c}} +[B]\left\{\sum_{n=0}^{\infty} E^n\right\}\Bigg|_{t-\frac{L-x}{c}-\frac{2n+1}{c}L-\frac{x'}{c}} \tag{81}$$

where $\{E\}$ vector denotes the excitation function and the space–time dependent matrices are given, as follows:

$$[A] = \int_{\Delta l_j}\int_{\Delta l_i} \frac{1}{4\pi R}\{f\}_j\{f\}_i^{\mathrm{T}}\,\mathrm{d}x'\,\mathrm{d}x \tag{82}$$

$$[A_1^*] = \int_{\Delta l_j}\int_{\Delta l_i} \frac{\dfrac{1}{\varepsilon_{\mathrm{rg}}}\cos\theta - \sqrt{\dfrac{1}{\varepsilon_{\mathrm{rg}}} - \sin^2\theta}}{\dfrac{1}{\varepsilon_{\mathrm{rg}}}\cos\theta + \sqrt{\dfrac{1}{\varepsilon_{\mathrm{rg}}} - \sin^2\theta}} \frac{1}{4\pi R*}\{f\}_j\{f\}_i^{\mathrm{T}}\,\mathrm{d}x'\,\mathrm{d}x \tag{83}$$

$$[B] = \frac{1}{2Z_0}\int_{\Delta l_j}\int_{\Delta l_i} \{f\}_j\{f\}_i^{\mathrm{T}}\,\mathrm{d}x'\,\mathrm{d}x \tag{84}$$

$$[C] = \int_{\Delta l_j}\int_{\Delta l_i} \frac{1}{4\pi R_0}\{f\}_j\{f\}_i^{\mathrm{T}}\,\mathrm{d}x'\,\mathrm{d}x \tag{85}$$

$$\left[C_1^*\right] = \int_{\Delta \mathrm{l}_j}\int_{\Delta \mathrm{l}_i} \frac{\dfrac{1}{\varepsilon_{\mathrm{rg}}}\cos\theta - \sqrt{\dfrac{1}{\varepsilon_{\mathrm{rg}}} - \sin^2\theta}}{\dfrac{1}{\varepsilon_{\mathrm{rg}}}\cos\theta + \sqrt{\dfrac{1}{\varepsilon_{\mathrm{rg}}} - \sin^2\theta}} \frac{1}{4\pi R_0^*}\{f\}_j\{f\}_i^{\mathrm{T}}\,\mathrm{d}x'\,\mathrm{d}x \tag{86}$$

$$[D] = \int_{\Delta \mathrm{l}_j}\int_{\Delta \mathrm{l}_i} \frac{1}{4\pi R_L}\{f\}_j\{f\}_i^{\mathrm{T}}\,\mathrm{d}x'\,\mathrm{d}x \tag{87}$$

$$[D_1^*] = \int_{\Delta \mathrm{l}_j}\int_{\Delta \mathrm{l}_i} \frac{\dfrac{1}{\varepsilon_{\mathrm{rg}}}\cos\theta - \sqrt{\dfrac{1}{\varepsilon_{\mathrm{rg}}} - \sin^2\theta}}{\dfrac{1}{\varepsilon_{rg}}\cos\theta + \sqrt{\dfrac{1}{\varepsilon_{\mathrm{rg}}} - \sin^2\theta}} \frac{1}{4\pi R_L^*}\{f\}_j\{f\}_i^{T}\,\mathrm{d}x'\,\mathrm{d}x \tag{88}$$

Having completed the space discretization procedure, the weighted residual approach is used for the time discretization procedure, as well.

Assuming that solution in time on the *i*th space segment can be expressed as:

$$I_i(t') = \sum_{k=1}^{N_t} I_i^k T^k(t') \tag{89}$$

where $I_i^k$ are the unknown coefficients and $T^{\mathrm{k}}$ are the time domain shape functions, and choosing the Dirac impulses as test functions, the recurrence formula for the space–time varying current can be written as:

$$I_{j_{|t_k}} = \frac{-\sum_{i=1}^{N_g}\left(\bar{A}_{ji} I_{i_{\left|t_k-\frac{R}{c}\right.}} - A^*_{ji_1} I_{i_{\left|t_k-\frac{R^*}{c}\right.}}\right) + g_{j_1}{}^*\big|_{\text{all retarded times}}}{A_{jj}} \tag{90}$$

where $N_{\mathrm{g}}$ denotes the total number of global nodes $A_{ji}$ are the global matrix terms, $g_{jl}{}^*$ is the whole right ride of the expression (81) containing the excitation and the currents at previous instants, while the overbar denotes that the self term is omitted.

Once the current distribution is obtained by solving the integral equation (74) via the GB-IBEM, the energy-measure integrals (76) and (77) can be evaluated.

First, the charge distribution is determined by solving the integral:

$$q = -\sum_{i=1}^{M}\sum_{k=1}^{N_t}\int_{\Delta t_k} \frac{\partial}{\partial x'}\{f\}_i^{\mathrm{T}}\{I\}_i \,\mathrm{d}t \tag{91}$$

where $M$ denotes the total number of segments, while $N_{\mathrm{t}}$ stands for the total number of time steps.

The solution of integral in eqn (91) is carried out analytically, and given in the form:

$$q = -\frac{1}{2v}\sum_{i=1}^{M}\sum_{m=1}^{N_t}(I_{i+1}^m + I_{i+1}^{m+1} - I_i^m - I_i^{m+1}) \tag{92}$$

The $H$-field energy measure is obtained by evaluating the integral:

$$W_I = \frac{\mu_0}{4\pi}\sum_{i=1}^{M}\int_{\Delta t_k} \frac{\partial}{\partial x'}(\{f\}_i^{\mathrm{T}}\{I\}_i)^2 \,\mathrm{d}x' \tag{93}$$

The solution is available in the closed form and is given by:

$$W_I = 10^{-7}\frac{\Delta x}{3}\sum_{i=1}^{M}\left[(I_i^k)^2 + I_i^k I_{i+1}^k + (I_{i+1}^k)^2\right], \quad k = 1, 2, \ldots, N_{\mathrm{t}} \tag{94}$$

The $E$-field energy is obtained from the integral:

$$W_q = \frac{1}{4\pi\varepsilon_r\varepsilon_0}\sum_{i=1}^{M}\int_{\Delta t_k}\frac{\partial}{\partial x'}(\{f\}_i^{\mathrm{T}}\{q\}_i)^2\,\mathrm{d}x' \tag{95}$$

for which the solution is then:

$$W_q = \frac{1}{4\pi\varepsilon_r\varepsilon_0}\frac{\Delta x}{3}\sum_{i=1}^{M}[(q_i^k)^2 + q_i^k q_{i+1}^k + (q_{i+1}^k)^2], \quad k = 1,2,\ldots,\ N_t \tag{96}$$

and the total energy measure is given by sum of $W_I$ and $W_q$.

### 3.4 Alternative time domain formulation via a simplified reflection/transmission coefficient

A transient analysis of a finite length wire embedded in a dielectric half-space and illuminated by the electromagnetic pulse (EMP) using a simplified reflection coefficient approach. A direct time domain formulation is based on the wire antenna theory and on the corresponding Hallen integral equations for half-space problems. The presence of a dielectric half-space is taken into account via the simplified reflection/transmission coefficient arising from the modified image theory. The Hallen equation is solved via the time-domain GB-IBEM and some illustrative numerical results are presented in this section.

The transient response obtained using the simplified reflection/transmission coefficient approach is compared to the results obtained via the Fresnel coefficients approach.

A simplified form of the earth–air reflection coefficient, based on the modified image theory, and proposed in [28] is given by:

$$\Gamma_{\mathrm{MOT}}^{\mathrm{ref}}(t) = \Gamma_{\mathrm{MOT}}^{\mathrm{ref}}\delta(t) \tag{97}$$

where $\Gamma_{\mathrm{MOT}}^{\mathrm{ref}}$ depends on the permittivity of the dielectric medium, only:

$$\Gamma_{\mathrm{MOT}}^{\mathrm{ref}} = \frac{1-\varepsilon_{\mathrm{rg}}}{1+\varepsilon_{\mathrm{rg}}} \tag{98}$$

A simplified form of the transmission coefficient, based on the modified image theory, proposed in [28] can be written, as follows:

$$\Gamma_{\mathrm{MOT}}^{\mathrm{tr}}(t) = \Gamma_{\mathrm{MOT}}^{\mathrm{tr}}\delta(t) \tag{99}$$

where $\Gamma_{\mathrm{MOT}}^{\mathrm{tr}}$, dependent only on the permittivity of the dielectric medium, is given by:

$$\Gamma_{\mathrm{MOT}}^{\mathrm{tr}} = \frac{2\varepsilon_{\mathrm{rg}}}{1+\varepsilon_{\mathrm{rg}}} \tag{100}$$

Substituting the relations (99) and (100) into eqn (71), for the case of normal incidence, it follows:

$$E_x^{\mathrm{tr}}(t) = \frac{2\varepsilon_{\mathrm{rg}}}{1+\varepsilon_{\mathrm{rg}}} E_x^{\mathrm{inc}}(t - t_0) \tag{101}$$

where $t_0 = d/v$ denotes the time delay.

Also, substituting eqns (97) and (98) into eqn (69), the resulting integral equations for the straight wire immersed in a dielectric medium becomes:

$$\int_0^L \frac{I(x', t - R/v)}{4\pi R}\,\mathrm{d}x' - \int_0^L \frac{1-\varepsilon_{\mathrm{rg}}}{1+\varepsilon_{\mathrm{rg}}} \frac{I(x', t - R^*/v)}{4\pi R^*}\,\mathrm{d}x'$$
$$= F_0\left(t - \frac{x}{v}\right) + F_L\left(t - \frac{L-x}{v}\right) + \frac{1}{2Z_{\mathrm{g}}} \int_0^L \frac{2\varepsilon_{\mathrm{rg}}}{1+\varepsilon_{\mathrm{rg}}} E_x^{\mathrm{inc}}\left(x',\ t - t_0 - \frac{|x-x'|}{v}\right)\mathrm{d}x' \tag{102}$$

The numerical solution of the space–time Hallen integral equation is obtained using the procedure presented in Section 2.3.

### 3.5 Computational examples

The first example is related to the straight wire of length $L = 5$ m and radius $a = 1$ cm embedded in the dielectric half-space with $\varepsilon_{\mathrm{r}} = 10$ at the depth $d = 1$ m. The wire is illuminated by the transmitted part of the EMP incident waveform:

$$E^{\mathrm{inc}}(t) = E_0(\mathrm{e}^{-at} - \mathrm{e}^{-bt}) \tag{103}$$

where the EMP parameters are: $E_0 = 52.5$ kV/m, $a = 4 \times 10^6$ s$^{-1}$ and $b = 4.78 \times 10^8$ s$^{-1}$.

The transient current induced at the wire center is shown in Fig. 8

The transient response obtained using the direct time domain approach seems to be in a satisfactory agreement with the results computed via the indirect frequency domain approach. The multiple reflections of the transient current from the wire ends are due to the reflected waves. This effect can be also observed in Figs 9–11.

Figure 9 shows the transient response of the same wire buried at various depths.

The curves shown in Fig. 9 for the transient current induced at the center of the wire embedded in the dielectric half-space at depth $d = 1$, 10 and 20 m represent time delayed waveforms due to the propagation delay necessary for the incident electric field to reach the wire. A slight amplitude and waveform variation as a function of depth indicate the minimal interface effect.

A slight proximity effect of the ground–air interface is visible for the case of the transient current induced along the wire placed at depth $d = 1$ m below ground, while only the time delay is noticeable for the curves related to the wires located at depth $d = 10$ and 20 m, respectively.

The initial delay of the first peak is caused by the arrival time of the incident field and strongly depends on the depth $d$. After that time the transient behavior of the incident current is the same.

Furthermore, Fig. 10 shows the transient current induced of the center of $L = 5$ m long wire buried at $d = 1$ m below the interface for the various values of permittivity. Thus, three typical values of relative dielectric constant are chosen; $\varepsilon_r = 10$ (ground), $\varepsilon_r = 55$ (brain permittivity at GSM (Global System for Mobile Communications) frequencies), $\varepsilon_r = 80$ (sea water). It can be observed from Fig. 10 that permittivity of the medium strongly affects the transient response of the wire embedded in the dielectric medium.

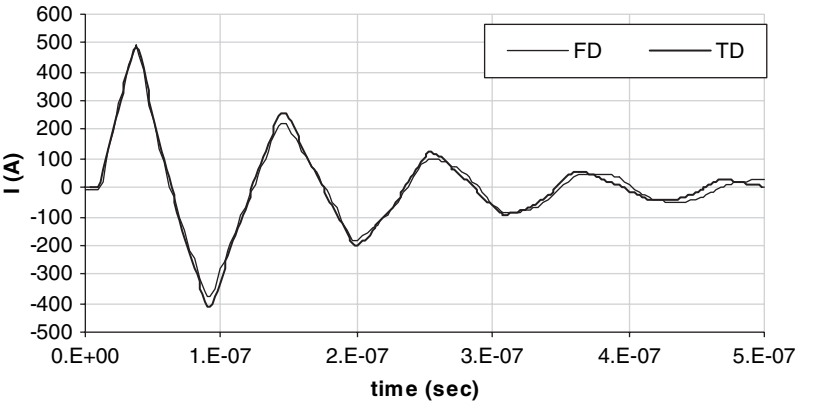


Figure 8: Transient current induced at the center of the straight wire ($L = 5$ m, $a = 1$ cm, $\varepsilon_r = 10$, $d = 1$ m).

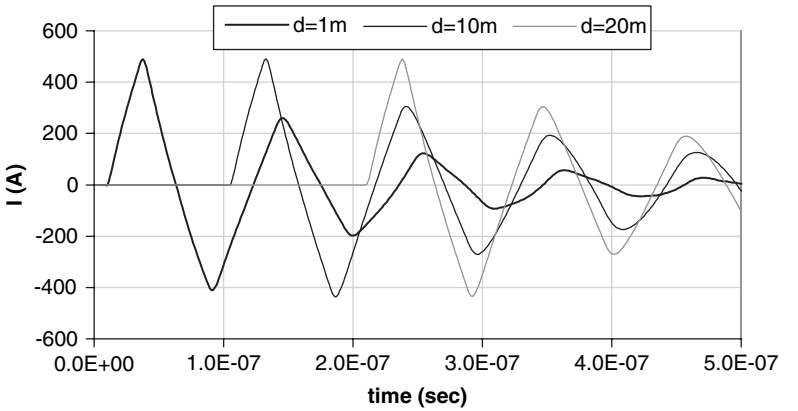


Figure 9: Transient current induced at the center of the straight wire ($L = 5$ m, $a = 1$ cm, $\varepsilon_r = 10$) for various depths.

As shown in Fig. 10 the initial delay of the transient waveform first peak is significantly influenced by the relative permittivity of a dielectric semi-infinite medium $\varepsilon_{rg}$. Also, time delay of the reflections from the wire free ends is influenced by the velocity of the propagation in the dielectric medium. Smaller the value of $\varepsilon_{rg}$, the greater is the velocity $v$ while the oscillation period is decreased.

Figure 11 shows the transient response of the straight thin wire of length $L = 50$ m and radius $a = 1$ cm embedded in the dielectric half-space with $\varepsilon_r = 10$ at the depth $d = 1$ m. The wire is illuminated by the EMP waveform (97). This transient response has been computed by means of the direct time domain and the indirect

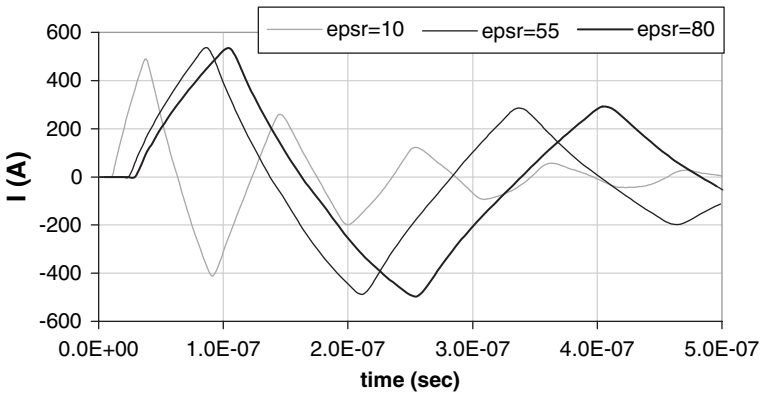


Figure 10: Transient response of the straight wires ($L = 5$ m, $a = 1$ cm) for various permittivity values.

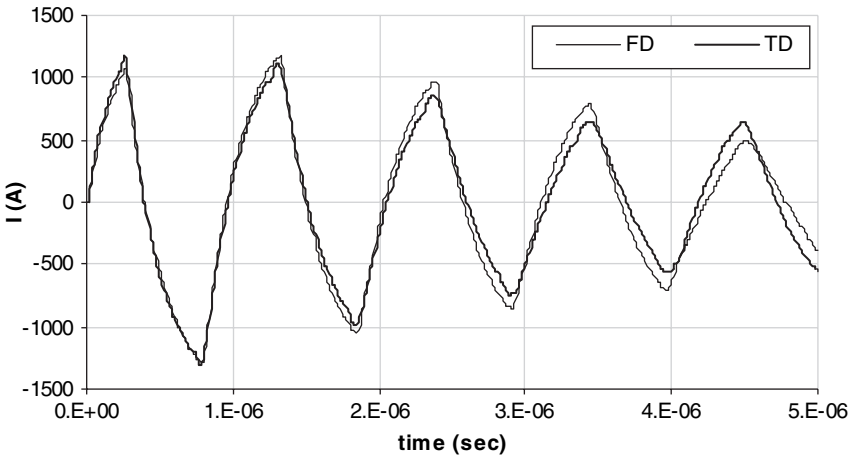


Figure 11: Transient current induced at the center of the straight buried wire ($L = 50$ m, $a = 1$ cm, $\varepsilon_r = 10$, $d = 1$ m).

frequency domain method, respectively. The numerical results obtained by the different approaches agree favorably again.

Comparison of the transient current from Fig. 11 with the current waveform from Fig. 8 clearly shows the influence of the wire length on the transient behavior.

It is also evident from Fig. 5 that the dominant effect to the transient behavior of the induced current along the line is due to the multiple reflections of the current wave from the line open ends.

There is a slight frequency shift in Figs 8 and 11 between the time domain and the frequency domain results, particularly for later time instants. Consequently, there are some points regarding the frequency domain modeling to be clarified.

The transients of highly resonant structures have very long duration while their related frequency spectra contain sharp peaks. Coarse frequency resolution cannot resolve the resonant points accurately thus resulting in errors in transient waveforms.

The problem of analyzing transients of highly resonant structures in the frequency domain is the inability to know beforehand the frequency resolution required for sampling the spectrum. Dynamic adaptive sampling can be used to overcome this problem and more details can be found in [4, 33]. An equivalent problem in analyzing transients in time domain is the inability to know the time duration of the waveform.

The related frequency spectrum of the impulse and the transient response of a 50 m long line immersed in a dielectric medium, with $\varepsilon_r = 10$ at depth $d = 1$ m is shown in Figs 12 and 13, respectively.

As it is visible from Figs 12 and 13, the frequency response spectra contain a number of peaks decreasing with frequency. Although the frequency range of these spectra is infinite, signal amplitudes for the frequencies higher than 50 MHz are low enough to be neglected. On the other hand, the location and the amplitude values of the first two peaks strongly affect the obtained transient waveform.

Therefore, it is very important for frequency samples to contain exact frequencies of the first two peaks. This could be achieved using the sufficiently fine frequency step (resulting in large number of samples) or by means of the dynamic

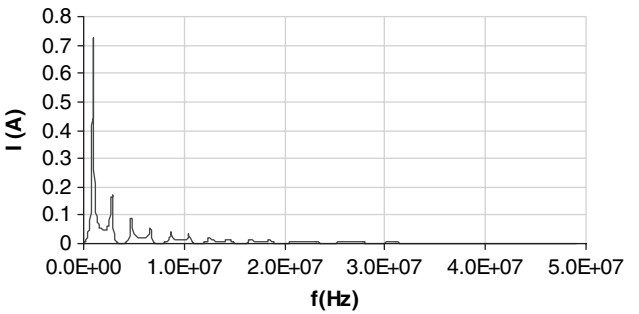


Figure 12: Frequency spectrum of the impulse response at the center of the straight wire ($L = 50$ m, $a = 1$ cm, $\varepsilon_r = 10$, $d = 1$ m).

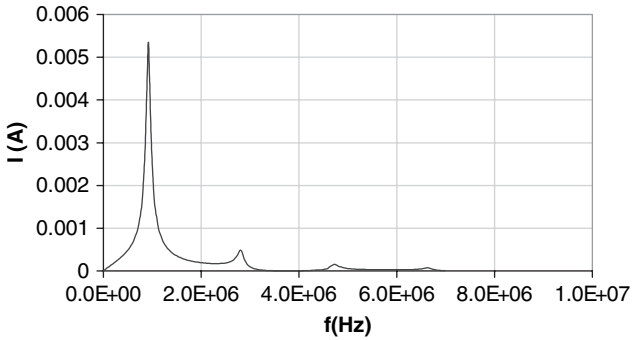


Figure 13: Frequency spectrum of the transient response at the center of the straight wire ($L$ = 50 m, $a$ = 1 cm, $\varepsilon_r$ = 10, $d$ = 1 m).

adaptive sampling technique presented in [31]. In this section a number of $N = 2^{15}$ samples over the frequency range of 50 MHz have been used in order to obtain a satisfactory convergence rate.

Since the current distribution evaluation for a single frequency takes around 30 s (depending on the computer speed), the calculation of current amplitude for each sample is obviously impossible. Thus, about 150 samples over the 50 MHz frequency range have been evaluated, while the rest of the samples have been interpolated using cubic splines.

The effect of the interface and the validity of the Fresnel reflection coefficient approximation in modeling the interface should be discussed, as well.

A relatively short wire ($L$ = 0.5 m) is chosen to describe the earth–air interface effect. Figure 14 shows the transient current induced at the center of 0.5 m long wire for various depths. As is obvious from Fig. 14, there is a slight variation in amplitude and waveform and time shift for depths $d$ = 0.25, 1 and 2 m. Only the curve for $d$ = 0.1 m clearly demonstrates the influence of the earth–air interface in both the amplitude and waveform of the actual transient response.

Figure 15 shows the behavior of the energy stored in the near field of the wire, i.e. it represents the decrease of the wire total energy with time, once the exciting pulse vanishes.

Figure 15 also demonstrates the absorbing effect of the dielectric half-space when the wire is brought closer to the interface.

The evaluation of the validity of the proposed model is not an easy task, even in the frequency domain, and even for the simplified case of a dielectric half-space. Generally, the validity of various approximations depends on the relationship between; the spectral content and the direction of the incident field, the electrical properties of the earth, and to a lesser extent the burial depth of the line. The computational aspects in the frequency domain modeling of thin wire antennas in the presence of a lossy half-space have been reported in a number of papers and among the most cited ones are references [15, 16].

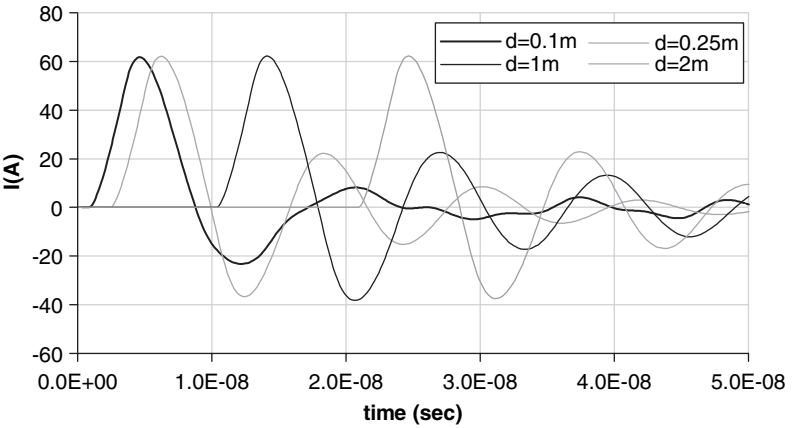


Figure 14: Transient current induced at the center of the straight wire ($L$ = 0.5 m, $a$ = 1 cm, $\varepsilon_r$ = 10) for various depths.

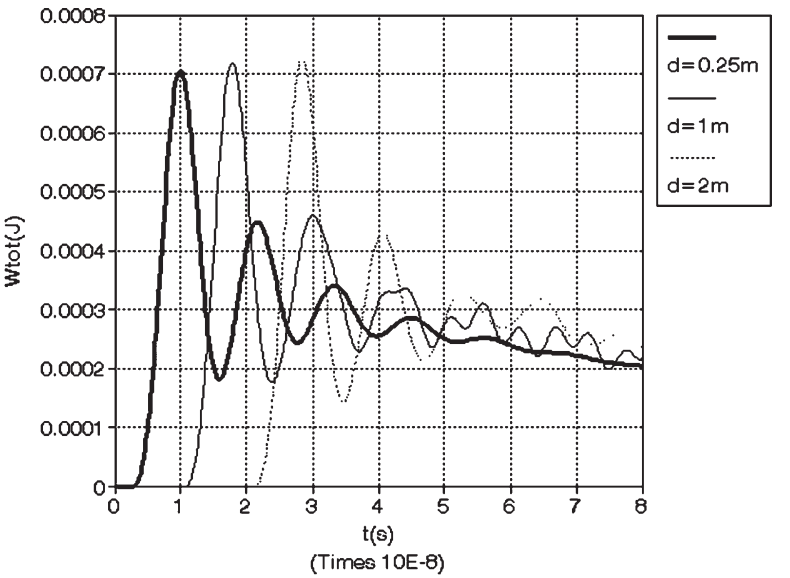


Figure 15: The measure of total energy ($W_{tot}$) as a function of time for various depths.

The frequency domain analysis of the buried wire scatterer has been carried out via the rigorous Sommerfeld integral [17], and via the approximate reflection coefficient approach [18], respectively, to account for the influence of the earth–air interface reflected field upon the straight wire scatterer current distribution.

The Sommerfeld integral approach has been found to be numerically stable and reliable for straight horizontal line brought to within $10^{-6}$ wavelengths of the interface [16, 17]. The rigorous and approximate results are in a very good agreement for depths greater or at least equal to [23]:

$$d \geq \frac{\lambda_0}{4\sqrt{\varepsilon_r}}, \quad \lambda_0 = \frac{c}{f} \tag{104}$$

As a rough guideline, the Fresnel reflection coefficient approach to account for the reflection from the earth–air interface has been found to produce results generally within 10% of those obtained using rigorous, but computationally very expensive, Sommerfeld integral approach.

Furthermore, for wire depths:

$$d \leq \frac{\lambda_0}{10\sqrt{\varepsilon_r}} \tag{105}$$

the qualitative dependence of the input admittance (obtained by using the reflection coefficient approach) upon depth is found to be generally correct, but these results primarily differ from the rigorous results due to a slight shift in the maxima with respect to depth.

Essentially, from the time domain point of view this condition should be satisfied for each component of the considered frequency spectrum.

It is also necessary to make at least a general trade-off between a dielectric half-space and an imperfectly conducting half-space. The absence of the ground conductivity (or at least low values of ground conductivity) causes strong resonance effect, which is particularly noticeable in Figs 11–13.

From the findings in the frequency domain the increasing ground conductivity is expected to decrease the response rapidly. In the realistic problems such as wire immersed inside sea water, ground probing or ground penetrating radar conductivity should not be neglected. The influence of the finite conductivity reduces the external electric field and influences the behavior of the induced current. The finite conductivity can also delay the initial field. However, the corresponding Green's function, which is responsible for the second effect, is much more complicated and has to be calculated via the Sommerfeld integral approach. In that case, one would need to perform additional integration in the Hallen equation and the problem would become tremendously time consuming.

To roughly estimate whether a dielectric half-space approximation of a dissipative half space can be used the absolute value of the refractive index of the earth should be examined.

This equation is given by

$$|n| = \sqrt{\varepsilon_{rg}^2 + \left(\frac{\sigma_g}{\omega\varepsilon_0}\right)^2} \tag{106}$$

Conductivity $\sigma$ should be at least an order of magnitude less than $\omega\varepsilon_0$ to be neglected.

For example, a reasonably dry earth, $\varepsilon_{rg} = 10$, in the frequency band from around 1 kHz to 1 MHz requires the conductivity $\sigma$ to vary from $10^{-6}$ to $10^{-4}$ S/m.

To sum up, the numerical results obtained via the different approaches agree satisfactorily, i.e. the maximum deviation between the results is around 6%.

The transient response of the single straight wire immersed in a dielectric half-space has been found to be influenced to a greater extent by the line length and the permittivity of a dielectric medium, and to a lesser extent by the burial depth.

The last set of numerical results deals with the transient analysis of a finite length wire immersed in a dielectric half-space using a simplified reflection/coefficient approach [29].

The computational example is related to the straight thin wire of length $L = 10$ m and radius $a = 6.74$ cm embedded in the dielectric half-space ($\varepsilon_r = 9$) at a certain burial depth $d$. The wire is illuminated by the transmitted part of the EMP incident waveform (103) where the EMP parameters are: $E_0 = 1.05$ kV/m, $a = 4 \times 10^6$ s$^{-1}$ and $b = 4.78 \times 10^8$ s$^{-1}$.

The transient current induced at the wire center, for various depths, computed via both the Fresnel and the simplified reflection/transmission coefficient is shown in Figs 16 and 17.

As in the case of the Fresnel coefficients approach, the evaluation of the validity of the proposed reflection/coefficient approximation is not an easy task, even for the case of a lossless dielectric half-space.

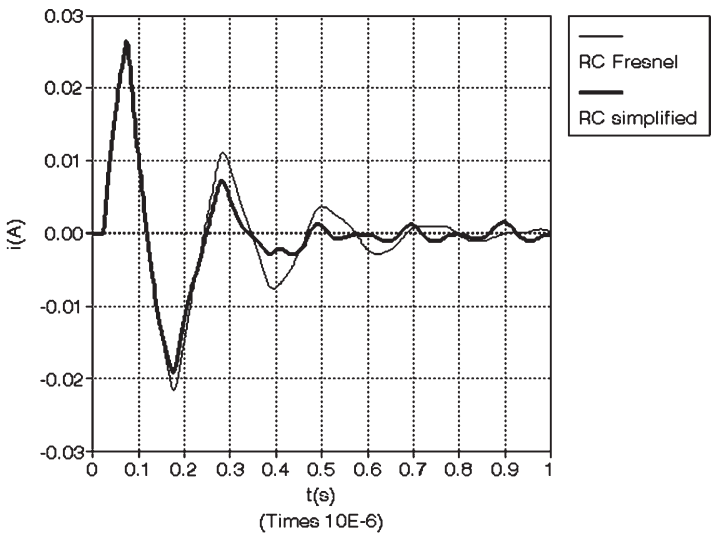


Figure 16: Transient current induced at the center of the straight wire ($L = 10$ m, $a = 6.74$ cm, $\varepsilon_r = 9$) at burial depth $d = 2.5$ m.

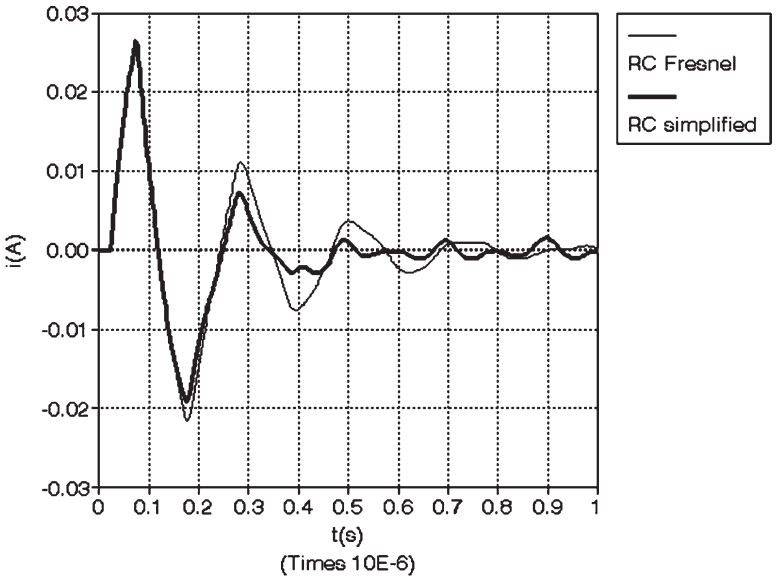


Figure 17: Transient current induced at the center of the straight wire ($L$ = 10 m, $a$ = 6.74 cm, $\varepsilon_r$ = 9) at burial depth $d$ = 5 m.

It is obvious from Figs 16 and 17 that the obtained numerical results via simplified reflection/coefficient approach agree satisfactorily with the results calculated via the Fresnel coefficients approach for earlier time instants and for increasing values of burial depth $d$.

## References

[1] Bridges, G.E., Transient plane wave coupling to bare and insulated cables buried in a lossy half-space. *IEEE Trans. EMC*, **37(1)**, pp. 62–70, 1995.

[2] Grcev, L.D. & Menter, F.E., Transient electromagnetic fields near large earthing systems. *IEEE Trans. Magnetics*, **32**, pp. 1525–1528, 1996.

[3] Tesche, F., Ianoz, M. & Carlsson, F., *EMC Analysis Methods and Computational Models*, John Wiley & Sons: New York, 1997.

[4] Poljak, D. & Tham, C.Y., *Integral Equation Techniques in Electromagnetics*, WIT Press: Southampton and Boston, 2003.

[5] Ianoz, M., Electromagnetic field coupling to lines, cables and networks, a review of problems and solutions. *Proc. Int. Conf. on Electromagnetics in Advanced Applications, ICEAA'95*, Turin, Italy, pp. 75–80, 12–15 September 1997.

[6] Tkatchenko, S., Rachidi, F. & Ianoz, M., High frequency electromagnetic field coupling to long terminated lines. *IEEE Trans. EMC*, **43(2)**, pp. 117–129, 2001.

[7] Tkatchenko, S., Rachidi, F. & Ianoz, M., Electromagnetic field coupling to a line of a finite length: theory and fast iterative solutions in frequency and time domains. *IEEE Trans. EMC*, **37(4)**, pp. 509–518, 1995.

[8] Poljak, D. & Roje, V., Time domain modeling of electromagnetic field coupling to transmission lines. *Proc. 1988 IEEE EMC Symposium*, Denver, USA, pp. 1010–1013, August 1997.

[9] Poljak, D., Tham, C.Y., McCowen, A. & Roje, V., Electromagnetic pulse excitation of multiconductor transmission lines. *ICEAA'99*, Turin, Italy, pp. 789–792, 13–17 September 1997.

[10] Poljak, D., Miller, E.K. & Tham, C.Y., Time domain energy measures for thin-wire antennas and scatterers. *IEEE Antennas & Propagation Magazine*, **44(1)**, pp. 87–95, 2002.

[11] Poljak, D., Tham, C.Y. & McCowen, A., Transient response of nonlinearly loaded wires in a two media configuration. *IEEE Trans. EMC*, **46(1)**, pp. 121–125, 2004.

[12] Degauque, P. & Zeddam, A., Remarks on the transmission approach to determining the current induced on above-ground cables. *IEEE Trans. EMC*, **30(1)**, pp. 77–80, 1997.

[13] Poljak, D., *Electromagnetic Modelling of Wire Antenna Structures*, WIT Press: Southampton, Boston, 2001.

[14] Poljak, D., New numerical approach in analysis of thin wire radiating over lossy half-space. *International Journal for Numerical Methods in Engineering*, **38(22)**, pp. 3803–3816, 1995.

[15] Miller, E.K., Poggio, A.J., Burke, G.J. & Selden, E.S., Analysis of wire antennas in the presence of a conducting half-space, Part II. The horizontal antenna in free space. *Canadian Journal of Physiscs*, **50**, pp. 2614–2627, 1972.

[16] Burke, G.J. & Miller, E.K., Modelling antennas near to and penetrating a lossy interface. *IEEE Trans. AP*, **32(10)**, pp. 1040–1049, 1984.

[17] Poljak, D. & Roje, V., The integral equation method for ground wire input impedance. *Integral Methods in Science and Engineering, Vol. I Analytic Methods*, eds C. Constanda, J. Saranen & S. Seikkala, Longman: New York, pp. 139–143, 1997.

[18] Poljak, D., Electromagnetic modeling of finite length wires buried in a lossy half-space. *Engineering Analysis with Boundary Elements*, **26**, pp. 81–86, 2002.

[19] Doric, V., Poljak, D. & Roje, V., Transient plane wave coupling to a finite length wire buried in a conductive ground. *Boundary Elements*, **XVII**, pp. 609–617, 2005.

[20] Poljak, D. & Brebbia, C.A., Indirect Galerkin–Bubnov boundary element method for solving integral equations in electromagnetics. *Engineering Analysis with Boundary Elements*, **28(7)**, pp. 771–777, 2004

[21] Ziemer, R.E. & Tranter, W.H., *Principles of Communications*, Houghton Mifflin Company: Boston and Toronto, 1995.

[22] King, R.W.P., Sforza, P.F. & Boak, T.I.S., The current in a parasitic antenna in a dissipative medium. *IEEE Trans. AP*, **22(6)**, pp. 809–814, 1974.

[23] Poljak, D. & Doric, V., Time domain modeling of electromagnetic field coupling to finite length wires embedded in a dielectric half-space. *IEEE Trans. EMC*, **47(2)**, pp. 247–253, 2005.

[24] Miller, E.K. & Landt, J.A., Direct time-domain techniques for transient radiation and scattering from wires. *Proc. IEEE*, **168(11)**, pp. 1396–1423, 1980.

[25] Miller, E.K., PCs for AP and EM reflections. *IEEE Antennas & Propagation Magazine*, **40(1)**, pp. 96–100, 1998; **41(2)**, pp. 92–95, 1997.

[26] Poljak, D., Miller, E.K., Tham, C.Y., Yoong, C., Antonijevic, S & Doric, V., Time domain analysis of the energy stored in the near field of multiple straight-wires above dielectric half-space. *Proceedings of the ICEAA*, Turin, September 2005.

[27] Poljak, D., Time domain analysis of the energy stored in the near field of finite length wires embedded in a dielectric half-space. *Proc. Int. Symp. on EMC*, *EMC Europe 2006*, Barcelona, Spain, pp. 982–987, 4–8 September 2006.

[28] Poljak, D. & Kresic, S., A simplified calculation of transient plane waves in a presence of an imperfectly conducting half-space. *Boundary Elements XXVII*, Orlando, pp. 541–549, 2005.

[29] Poljak, D. & Kovac, N., Transient analysis of a finite length line embedded in a dielectric half-space using a simplified reflection/transmission coefficient approach. Submitted to *ICEAA 2007 Conference*, Turin, Italy, September 2007.

[30] Rao, S.M., Sarkar, T.K. & Dianat, S.A., A novel technique to the solution of transient electromagnetic scattering from thin wires. *IEEE Trans. AP*, **34**, pp. 630–634, 1986.

[31] Tijhuis, A.G., Peng, Z.Q. & Bretones, A.R., Transient excitation of a straight thin-wire segment: a new look at an old problem. *IEEE Trans. AP*, **40(10)**, pp. 1132–1146, 1992.

[32] Poljak, D., Transient response of resistively loaded straight thin wire in half-space configuration. *Journ. Elctromagn. Waves and Applic.*, **12(6)**, pp. 775–787, 1997.

[33] Tham, C.Y., McCowen, A., Towers, M.S. & Poljak, D., Dynamic adaptive sampling technique in frequency-domain transient analysis. *IEEE Trans. EMC*, **44(4)**, pp. 522–528, 2002.